# Imidazoporphyrins as supramolecular tectons: synthesis and self-assembly of zinc 2-(4-pyridyl)-1H-imidazo[4,5-b]porphyrinate

Inna A. Abdulaeva, Kirill P. Birin, Anna A. Sinelshchikova, Mikhail S. Grigoriev, Konstantin A. Lyssenko, Yulia G. Gorbunova, Aslan Yu. Tsivadze, Alla Bessmertnykh-Lemeune

CrystEngComm

Accepted Manuscript

This article can be cited before page numbers have been issued, to do this please use: K. P. Birin, A. Inna, A. A. Sinelshchikova, M. S. Grigoriev, K. A. Lyssenko, Y. G. Gorbunova, A. Y. Tsivadze and A. Bessmertnykh-Lemeune, *CrystEngComm*, 2019, DOI: 10.1039/C8CE01992D.




ROYAL SOCIETY OF CHEMISTRY

rsc.li/crystengcomm

ROYAL SOCIETY OF CHEMISTRY View Article Online
DOI: 10.1039/C8CE01992D

Journal Name

ARTICLE

# Imidazoporphyrins as supramolecular tectons: synthesis and self-assembling of zinc 2-(4-pyridyl)-1*H*-imidazo[4,5-*b*]porphyrinate

Received 00th January 20xx,
Accepted 00th January 20xx

DOI: 10.1039/x0xx00000x

www.rsc.org/

Inna A. Abdulaeva,[a,b] Kirill P. Birin,[a,*] Anna A. Sinelshchikova,[a] Mikhail S. Grigoriev,[a] Konstantin A. Lyssenko,[c] Yulia G. Gorbunova,[a,d] Aslan Yu. Tsivadze,[a,d] Alla Bessmertnykh-Lemeune[b,*]

5,10,15,20-Tetramesityl-2-(4-pyridyl)-1*H*-imidazo[4,5-*b*]porphyrin (**PyPor**) bearing the pyridine donor site connected to the tetrapyrrolic macrocycle by the rigid imidazole linker was prepared in high yield by the condensation of the corresponding 2,3-dioxochlorin and 4-formylpyridine in the presence of ammonium acetate. After the insertion of a metal ion capable of the metal-ligand axial coordination, namely Zn(II), this compound afforded self-complementary porphyrin **PyPorZn** which is suitable for self-assembly. In the crystals, this complex exists as a zig-zag polymer formed through the axial coordination of the pyridine nitrogen atom to the zinc ion of the neighbouring porphyrin molecule. The Zn atoms adopt a distorted tetragonal pyramidal environment and the pyridine rings significantly deviate from the orthogonal orientation to the mean $N_4$ plane of the adjacent macrocycle ($C_{para}$–$N_{Py}$–Zn angle is equal to 148°). This distortion was analysed by using DFT calculations of zinc 5,10,15,20-tetraphenylporphyrinate-pyridine complex (**TPPZn–Py**). The energy and the geometry of **TPPZn–Py** was calculated varying a tilt of pyridine ligand. The change of $C_{para}$–$N_{Py}$–Zn angle from 180° to 150° induces a small increase (within 1.5 kcal/mol) of the total energy of the complex. Such small increase can be easily compensated by the intermolecular CH···H and CH···π interactions in the crystals. Self-assembly of **PyPorZn** in non-coordinating solvents was also investigated by NMR and UV–vis spectroscopies. In contrast to nickel complex **PyPorNi**, the zinc complex exists in $10^{-4}$ M solution in toluene and chloroform as a mixture of short linear oligomers. These oligomers dissociate affording the monomer species upon heating, dilution or addition of a substituting ligand.

## Introduction

The synthesis and investigation of β-functionalized porphyrins emerged as a priority of porphyrin chemistry long ago[1,2] as β-substituted tetrapyrrolic macrocycles are widely used by living systems for optimal organization of different vital processes such as photosynthesis, transport of small molecules and catalytic oxidative transformations. In order to get deeper insight into these processes and to design artificial molecules and materials which exhibit similar or even higher efficiency in these processes, the development of simple and selective methods for the preparation of β-substituted porphyrins is of fundamental importance. However, synthetic approaches to these compounds are still laborious and time-consuming. Along these lines, many efforts have been devoted to the investigation of annulation reactions, and porphyrins fused with heterocyclic rings were identified as promising targets for the functionalization of β-pyrrolic positions of the porphyrin macrocycle. The introduction of π-conjugated systems fused with the aromatic core can deeply modify the electronic properties of the porphyrin macrocycle.[3,4] In contrast, the annulation of the imidazole ring does not contribute to the extension of the porphyrin π-system significantly.[5] Therefore, imidazo[4,5-*b*]porphyrins are of interest for the preparation of the modular porphyrin derivatives, arrays and conjugates. For example, imidazo[4,5-*b*]porphyrins bearing N-heterocyclic carbene fragment (NHC) at the periphery of the macrocycle[6–11] were prepared from derivatives unsubstituted at position 2 of the imidazole ring which are available by the condensation of β,β'-diaminoporphyrins and orthoformate.[10,11] The rhodium(II) and palladium(II) complexes with these porphyrin-modified NHCs exhibit remarkable catalytic activity in the ring-opening polymerization of L-lactide and the Mizoroki-Heck cross-coupling reaction, respectively.[12,13]

Fused porphyrins containing a 2-functionalized imidazole ring can be easily prepared by the condensation of β-dioxochlorins with aromatic aldehydes in the presence of ammonium acetate.[14–16] A wide range of derivatives bearing versatile terminal functions both at the tetrapyrrolic macrocycle and in the imidazole ring were prepared according to this procedure. Moreover, these compounds can also be obtained in high yields from β,β'-diaminoporphyrins and aldehydes that opens additional possibilities for their structural tuning.[17]

[a] A.N. Frumkin Institute of Physical Chemistry and Electrochemistry RAS, 119071, Leninsky pr., 31, building 4, Moscow, Russian Federation.
[b] Institut de Chimie Moléculaire de l'Université de Bourgogne, UMR CNRS 6302, Université Bourgogne Franche-Comté, 9 Avenue Alain Savary, 21078 Dijon, France.
[c] Department of Chemistry, Lomonosov Moscow State University, 119992 Moscow, Russian Federation.
[d] N.S. Kurnakov Institute of General and Inorganic Chemistry RAS, 119991, Leninsky pr., 31, Moscow, Russian Federation.
Electronic Supplementary Information (ESI) available: crystallographic data, information on quantum-chemical calculations and additional spectra. See DOI: 10.1039/x0xx00000x

Preliminary investigations of 2-functionalized imidazoporphyrins have shown that these compounds exhibit remarkable photophysical properties and represent useful mimics of natural systems involved in the photosynthesis.[18–21] These compounds are also promising for biomedical applications.[15] Imidazoporphyrins bearing terminal donor sites can serve as molecular tectons for the preparation of supramolecular systems. However, supramolecular chemistry of imidazoporphyrins is still scarcely studied. To the best of our knowledge, the only tetrakis(3,5-di-*tert*-butylphenyl)porphyrin fused with two (4-pyridyl)-substituted imidazole rings was explored as a guest molecule trapped into the cavity of a semi-rigid inner-functionalized U-shaped bisporphyrin by coordination bonding in $CH_2Cl_2$ solution.[22]

In our pursuit of new building blocks for self-complementary coordination of porphyrins,[23–28] in this article we address a question whether imidazoporphyrins may form self-assemblies in solid state and in solution. Pyridine-functionalized porphyrins[29–34] including chiral derivatives[35] have been widely explored in crystal engineering as the pyridine nitrogen atom is capable of strong coordination binding to many transition and main group metal ions. Changing the position of the nitrogen atom at the pyridine ring, the number of pyridine substituents and adding other coordination sites at the periphery of the macrocycle, the structural organization of supramolecular associates can be rationally tuned and adapted to desirable macroscopic properties of the solid materials.[29,36] Moreover, the distance between the metal centres and the nitrogen donor atoms as well as the mutual orientation of donor sites at the macrocycle periphery influence the structure of supramolecular associates.[35–39] However, only assembly of *meso*-pyridyl-substituted porphyrins was widely investigated since the synthesis of β-functionalized derivatives and their crystallization are difficult tasks. To the best of our knowledge, only the self-assembly of 2-(2-pyridyl)-5,10,15,20-tetra-substituted-porphyrins (**2PyZn**) was investigated in solutions.[40] It is also worth emphasizing, that all native supramolecular systems involving tetrapyrrolic macrocycles consist of β-functionalized derivatives while biomimetic studies of the self-assembly of β-substituted porphyrins are still limited to a few examples.[41]

Herein, we reveal the prospects of imidazo[4,5-*b*]porphyrins as tectons for crystal engineering. Zinc(II) imidazoporphyrinate **PyPorZn** bearing 4-pyridyl moiety at position 2 of the imidazole ring was successfully prepared and investigated by single crystal X-ray diffraction. 1D coordination polymer is formed in the crystals of **PyPorZn** owing to coordination binding of pyridyl groups to the Zn centres. The quantum-chemical calculations were performed in order to explain the unusual orientation of the pyridine unit in the coordination sphere of the zinc(II) atom. Finally, the solution behaviour of **PyPorZn** was explored to get deeper insight into the stability of the associates and to compare the self-assembly of this compound to that of earlier reported self-complementary porphyrins **2PyZn** bearing 2-pyridyl fragment at the β-position of tetrapyrrolic macrocycle.

## Results and discussion

View Article Online
DOI: 10.1039/C8CE01992D

Among the methods reported for the preparation of imidazoporphyrins,[14,15,17] we have chosen the condensation of 2,3-dioxochlorin and 4-formylpyridine in the presence of ammonium acetate (Scheme 1).[15] The free-base porphyrin **PyPor** was synthesized in 61% yield and further converted into the zinc and nickel complexes **PyPorZn** and **PyPorNi**. Zinc complex **PyPorZn** was expected to form supramolecular associates through the formation of intermolecular $Zn\cdots N_{Py}$ bonds, while Ni(II) complex **PyPorNi** was used as a reference monomer, since self-assembled Ni porphyrins are unknown to our knowledge. To this end, the free-base porphyrin **PyPor** was treated with $Zn(OAc)_2$ in $CHCl_3$/MeOH mixture at ambient temperature to afford the corresponding Zn(II) complex quantitatively (Scheme 1).[28] The synthesis of Ni(II) complex **PyPorNi** was performed upon reflux of **PyPor** and $Ni(acac)_2$ in toluene.[17] The obtained compounds were isolated and purified by column chromatography and characterized by $^1$H NMR and UV–vis spectroscopies as well as high resolution ESI mass spectrometry.

We succeeded in growing single crystals of **PyPorZn** by slow diffusion of methanol or ethylacetate into a toluene solution of the complex and performed their X-ray structural analysis (Figure 1 and S1, Figure 2 and S2). The complex is crystallized with two toluene molecules per each porphyrin in the monoclinic $P2_1/c$ space group. There are only two examples of imidazoporphyrins in CSD and both compounds contain 2-unsubstituted imidazole ring.[8,11] Thus **PyPorZn** is the first example of structurally characterized self-assembled 2-substituted imdazoporphyrins.

In the crystals of **PyPorZn** the zinc atom adopts a square-pyramidal coordination formed by four nitrogen atoms of the porphyrin core ($Zn–N_{Por}$ distances are 2.048(3)–2.078(3) Å) and the pyridyl nitrogen atom of the neighbouring molecule ($Zn–N_{Py}$ distance is 2.183(3) Å). The axial coordination of the pyridyl fragment to the zinc centre results in the displacement of this atom from the mean porphyrin $N_4$ plane by 0.286(1) Å which is comparable to that observed in other pentacoordinated zinc porphyrinates reported in CSD (0.25–0.35 Å).[42–44]

The imidazole cycle is planar. The hydrogen atom on imidazole nitrogen N(6) was located from difference Fourier map and its location was confirmed by the values of bond lengths (Figure 1). The bonds between N(6) and neighbouring carbon atoms are about equal (C(3)–N(6) = 1.368(4) Å, C(21)–N(6) = 1.366(4) Å) while for N(5) atom one of C–N distances is significantly shorter than the other

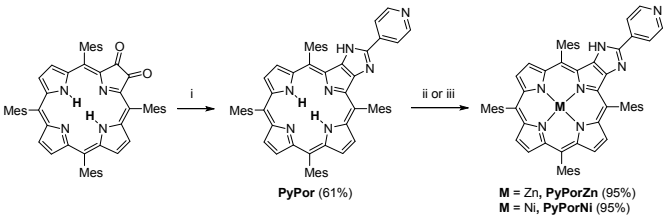


Scheme 1. The synthesis of imidazoporphyrin **PyPor** and complexes **PyPorNi** and

**PyPorZn**. i: 4-formylpyridine, $NH_4OAc$, TFA, $CHCl_3$, reflux; ii: $Zn(OAc)_2$, $CHCl_3$/MeOH, rt; iii: $Ni(acac)_2$, toluene, reflux.

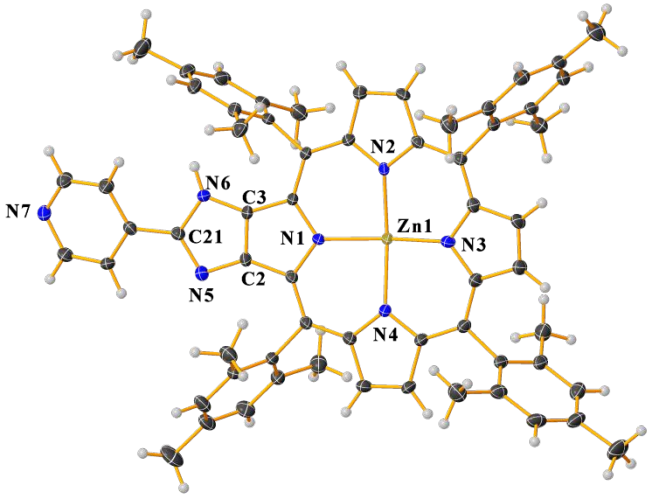


Figure 1. Molecular structure of **PyPorZn·2C$_6$H$_5$CH$_3$**. Two toluene molecules are omitted for clarity. Thermal ellipsoids are at the 50% probability level. Selected bond lengths (Å): Zn(1)–N(1) = 2.048(2); Zn(1)–N(2) = 2.073(2); Zn(1)–N(3) = 2.067(3); Zn(1)–N(4) = 2.078(3); Zn(1)–N(7)$^1$ = 2.183(3); $^1$2-X,-1/2+Y,3/2-Z.

(C(21)–N(5)=1.341(4) and C(2)–N(5)=1.386(4) Å).

The fused imidazole and pyrrole rings are virtually coplanar and two mean planes of these heterocycles form a dihedral angle of 2.4°. The porphyrin macrocycle is also virtually planar and significant deviations of $C_\beta$ atoms from the mean porphyrin $N_4$ plane is observed only for carbon atoms fused with imidazole fragment (–0.243(5) Å for C(2)). As a result, the condensed pyrrole-imidazole fragment is slightly skewed with respect to the mean porphyrin $N_4$ plane. The dihedral angle between the imidazole and the porphyrin $N_4$ plane is equal to 8.1° and similar to those observed in an previously reported bis(imidazo)porphyrin (9.2° and 11.4°).[11] The pyridine fragment is twisted with respect to the porphyrin core and the imidazole ring. The dihedral angle between the pyridine cycle and the imidazole plane is 17.8° that considerably exceeds the typical values for (2-pyridyl)-benzimidazoles (1–10°).[45,46] It can be explained by the steric hindrance induced by two aryl substituents located at the nearest *meso*-positions of the porphyrin macrocycle.

In the studied crystals, complex **PyPorZn** forms 1D polymer chains in which porphyrin molecules are connected owing to coordination binding of the pyridine nitrogen atom to the zinc atom of the neighbouring species (Figure 2). Surprisingly, in these polymer chains the axial pyridyl substituent is tilted with respect to the mean porphyrin $N_4$ plane. In fact, the pyridyl substituent is expected to be orthogonal to this plane and the angle defined by Zn atoms, pyridyl N and *para*-C atoms ($C_{para}$–$N_{Py}$–Zn) should be close to 180°.[47,48] In the crystals of **PyPorZn·2C$_6$H$_5$CH$_3$** this angle (C(22)–N(7)–Zn(1)) is equal to 147.9(1)° (Figure 3). Such deviation of the pyridine fragment in the axial position from the orthogonal to the $N_4$ plane are quite rare but already reported for porphyrin complexes (Figure S2). For instance, the $C_{para}$–$N_{Py}$–Zn angles of 148.2°–154.5° were observed in supramolecular complexes with pentacoordinated

View Article Online
DOI: 10.1039/C8CE01992D

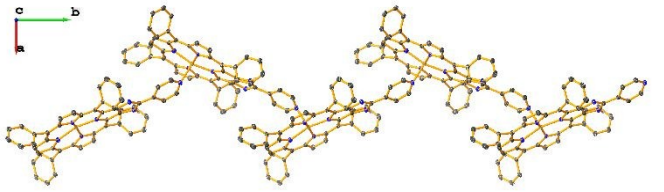


Figure 2. 1D polymer chain of **PyPorZn·2C$_6$H$_5$CH$_3$**. Thermal ellipsoids are drawn at the 50% probability level. Hydrogen atoms and methyl groups of methyl substituents are omitted for clarity.

zinc atoms[49,50] and zinc porphyrinate having hexacoordinated zinc centre[51] (Figure S3).

It is worth mentioning that the maximal tilting of the pyridine fragment was observed in the supramolecular complexes in which the 4-pyridine ring serves for formation of supramolecular architectures. In discrete porphyrin complexes with pyridine ligand, the minimum value of the $C_{para}$–$N_{Py}$–Zn angle appeared to be 155.8°.[52]

The dihedral angle between adjacent mean $N_4$ planes in 1D chain **[PyPorZn]$_n$** is 48.7°. The zig-zag polymer chain extends in the [010] direction with the repeating unit corresponding to the crystallographic *b* parameter. Such zig-zag motif is typical for *meso*-pyridylporphyrinates.[43] However the mutual orientation of neighbouring porphyrin moieties differs from that of the *meso*-pyridyl-substituted porphyrin **ZnMPyTPP** where the mean $N_4$ planes are almost orthogonal (86.5°). The Zn···Zn distance between adjacent molecules of **PyPorZn** is increased compared to *meso*-pyridyl-substituted porphyrin **ZnMPyTPP** (9.806 Å and 12.216 Å in **ZnMPyTPP** and **PyPorZn·2C$_6$H$_5$CH$_3$**, respectively) due the presence of the imidazole linker in complex **PyPorZn**.

The crystal packing of **PyPorZn·2C$_6$H$_5$CH$_3$** was analysed using the ToposPro program package by calculating the molecular Voronoi-Dirichlet polyhedra boundary surfaces. The strongest interactions are observed between adjacent porphyrin moieties within 1D chains (Table S4a). The summary of multiple C···H, C···C and H···H van der Waals contacts between the chains are given in Table S5. The porphyrin chains bonded through the strongest contacts form a pseudo-layer in (100) crystallographic direction (Table S4b).

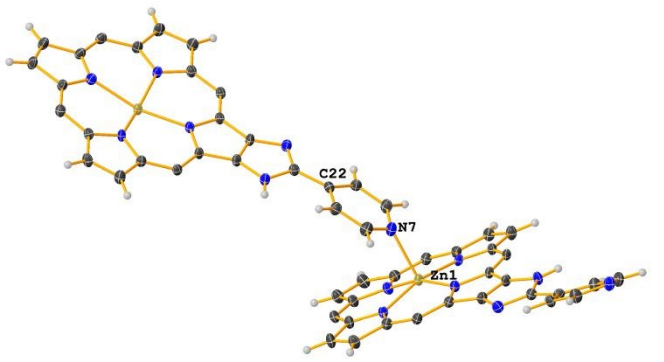

View Article Online DOI: 10.1039/C8CE01992D

Figure 3. The dimeric fragment of the polymer chain **[PyPorZn]$_n$**, mesityl substituents are omitted for clarity. Thermal ellipsoids are at the 50% probability level. Selected angle (°): C(22)–N(7)–Zn(1) = 147.9(1).

Considering all meaningful contacts, the crystal can be regarded as a 3D pseudo-framework (Table S4c) in which each porphyrin molecule is surrounded by seven porphyrin species. The simplified net of this framework is an uninodal topological net **vmr** (http://rcsr.net/nets/vmr) which is frequently observed in the crystals (1965 examples including 6 porphyrins with CSD refcodes EYIQAF, GICCAX, KAXNEC, MUMGAD, SOXQOL, WAWVEX).

Next, DFT calculations were applied for the analysis of the structure of **PyPorZn**. For better understanding of the origin of the pyridine ligand distortion from the orthogonal orientation to the $N_4$ plane as well as its influence on the energy of the Zn–$N_{Py}$ bond, we have performed DFT PBE0 calculations of a model compound, namely – zinc 5,10,15,20-tetraphenylporphyrinate with an axially coordinated pyridine ligand **TPPZn–Py** (Table S6). The choice of the PBE0 functional was based on the recent article in which errors of various DFT functionals in the reproduction of the exact electron density and energy were discussed.[53] The geometry of **TPPZn–Py** was optimized using a very tight optimization criteria and empirical dispersion corrections on the total energy[54] with the Becke-Johnson damping (D3).[55]

Optimization of the **TPPZn–Py** geometry expectedly leads to the $C_{para}$–$N_{Py}$–Zn angle of 180° with the Zn–$N_{Py}$ distance equals to 2.187 Å. The Zn–$N_{Por}$ bond lengths are ranging from 2.068 Å to 2.187 Å. The energy of the Zn–$N_{Py}$ bond in **TPPZn–Py** was estimated using the topological analysis of the electron density distribution function ρ(r) within Bader's quantum theory of "Atoms in Molecule'' (QTAIM) theory.[56] Using the AIM formalism, one can distinguish binding interatomic interactions from all other contacts. When the distribution of ρ(**r**) in molecule or crystal is known, it is possible to answer the question whether the bonding interaction is present or not by the search of the bond critical point (3,–1) and to predict the energy of weak intermolecular interactions ($E_{cont}$) with a high accuracy on the basis of the potential energy density function v(**r**) – the correlation suggested by Espinosa et al. (CEML).[57] Recently, physical interpretation of CEML was suggested[58] and it was shown that the correlation is also valid for coordination bonds Gd–X (X = O, N, Cl)[59], Au–P[60], Pd–C[61], Ru···($C_5H_5$).[62]

According to the critical point (CP) search of ρ(r), CP (3,–1) in **TPPZn–Py** are located not only for all expected bonds but also for weak C–H···N interactions (H···N = 2.558 Å) between the pyridine fragment and nitrogen atoms of the porphyrin core (Figure S4) that is in agreement with the presence of short contacts in the structure of **PyPorZn** (Figure 3). Expectedly, all Zn–N bonds are characterized by the positive value of $\nabla^2\rho(\mathbf{r})$ (5.71–7.9 e Å$^{-5}$) and the negative electron energy density ($h_e(r)$) (–0.013 – –0.006 a.u.) in CP (3,–1) and, therefore, correspond to the intermediate type of interatomic interactions. In contrast, all C–C, C–H and C–N bonds are characterized by both negative $\nabla^2\rho(\mathbf{r})$ and $h_e(r)$ in CP (3,–1) and thus correspond to the shared type of interatomic interactions. Finally, the C–H···N interactions are found to be closed-shell interactions.

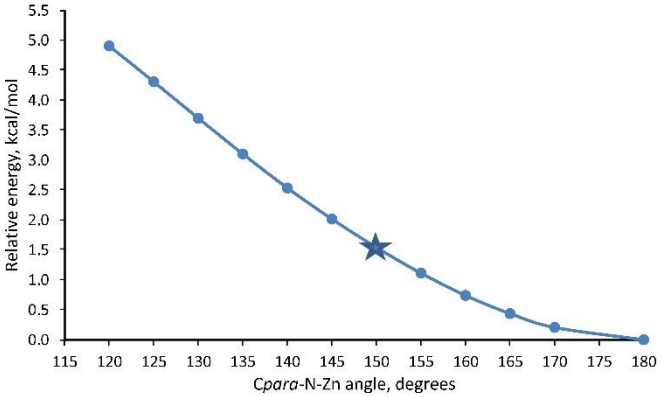


Figure 4. Variation of the relative energy (kcal/mol) of **TPPZn–Py** as the function of $C_{para}$–$N_{Py}$–Zn angle according to PBE1PBE/def-2-TZVP calculation. The point corresponding to the experimental value is shown by star.

The energies of Zn–$N_{Por}$ and Zn–$N_{Py}$ bonds according to CEML are equal to 33.5–33.8 and 22.48 kcal/mol, respectively, while the above-mentioned C–H···N contact is 1.8 kcal/mol. Thus, the total energy of interaction of pyridine with Zn-porphyrin moiety is equal to 26.0 kcal/mol. The estimation of the energy of Zn–$N_{Por}$ bonds is challenging in comparison with the calculations of the energy of the Zn–$N_{Py}$ bond, which can be evaluated as the difference of the total energy of the **TPPZn–Py** and the sum of total energies of pyridine and the zinc 5,10,15,20-tetraphenylporhyrinate possessing the same geometry as that of **TPPZn–Py** complex. Considering the counterpoise correction, this value is equal to 22.33 kcal/mol that is rather close to the above mentioned value calculated according to the CEML method. It indicates that the proposed approach can be used for the qualitative estimations of all Zn–N bonds in this system.

The relaxed potential energy scan along the $C_{para}$–$N_{Py}$–Zn angle coordinate has revealed that the energy of **TPPZn–Py** increases by only 5 kcal/mol upon the decrease of $C_{para}$–$N_{Py}$–Zn angle from 180 to 120° in 5° steps (Figure 4). Moreover, for the experimental value of $C_{para}$–$N_{Py}$–Zn (which is ca. 150°) the energy is higher by only 1.5 kcal/mole with respect to the energy minima. The analysis of molecular geometry has revealed that upon the decrease of $C_{para}$–$N_{Py}$–Zn angle the Zn–$N_{Py}$ bond length increases from 2.187 up to 2.457 Å, while the Zn–$N_{Por}$ distances decrease from 2.069 down to 2.056 Å (Table S7). For the $C_{para}$–$N_{Py}$–Zn angle of 150°, the Zn–$N_{Py}$ distance equals to 2.234 Å while the Zn–$N_{Por}$ bond lengths are in the range of 2.058–2.0708 Å. Notably, both in the crystal and in the isolated molecule the tilt of the pyridine ring leads to the significant nonequivalence of the Zn–$N_{Por}$ bond lengths with substantial shortening of those which are located in the opposite position against the direction of pyridine tilting. This dissymmetry is probably caused by steric effects of *meso*-mesityl substituents.

Thus, we can conclude that the inverse relation of Zn–N bond lengths for the porphyrin core and the pyridine ring leads to the compensation of Zn–$N_{Py}$ bond weakening by strengthening of

View Article Online
DOI: 10.1039/C8CE01992D



$Zn–N_{Por}$ ones (Table S6). This result can be illustrated by using the calculated according CEML values of Zn–N bond energy for different $C_{para}–N_{Py}–Zn$ angles. Thus, the energy of the $Zn–N_{Py}$ bond within the range of the experimentally observed values (180–145°) decreases from 22.5 to 17.1 kcal/mol, while the total energy of $Zn–N_{Por}$ bonds increases from 134.7 up to 136.4 kcal/mol that qualitatively coincide with the variation of relative energy of **TPPZn–Py** (Table S7). Analysis of the atomic charges obtained by the integration of atomic basis have revealed that the charge of Zn(1) is independent on the $C_{para}–N_{Py}–Zn$ angle and equals to 1.32 e. The total charge of pyridine fragment is also independent on the $C_{para}–N_{Py}–Zn$ angle and varies from 0.07 to 0.04 e.

Taking into account the energy of the above mentioned C–H···N interaction and the presence of weak C–H···H, C–H···π contacts between the methyl groups and the pyridine fragment in the crystals of **PyPorZn•2C$_6$H$_5$CH$_3$**, we can assume that the tilt of the pyridine ring up to 148°can stabilize the crystals.

Regarding the rigidity of this molecule, the thermally induced shortening of the weak contacts with clearly flat potentials can lead to an easy break of $Zn–N_{Py}$ bonds upon heating in solution. However, the positive role of the extra-coordination of Zn atoms by solvent molecules in this process should also be considered.

Going further, the self-assembly of complex **PyPorZn** in solution was explored. These investigations were performed using $^1$H NMR and UV–Vis techniques by revealing the influence of the complex concentration, temperature and the presence of a competing N- or O-donor ligands capable of the axial coordination to the central zinc atom.

The $^1$H NMR spectrum of $10^{-4}$ M solution of **PyPorZn** in $CDCl_3$ is significantly broadened while the spectra of the free-base porphyrin **PyPor** and nickel complex **PyPorNi** reveal well-defined sets of all expected resonances (Figures S5 and S6). The observed signal broadening can be reasonably attributed to the self-assembly process proceeding through labile $N_{Py}–Zn$ binding which was also observed in the crystals of **PyPorZn•2C$_6$H$_5$CH$_3$** and also reported for complex **2PyZn** in solution.[40] The addition of a competing ligand to the studied solution should suppress this self-assembly leading to a well-resolved spectrum of the complex. Pyridine-$d_5$ was chosen as a substituting ligand and added portionwise to the studied solution (Figure 5). After addition of only 1 vol% of pyridine-$d_5$, the signals of porphyrin β-protons appear as a set of expected resonances, while the signals of other protons remain broadened. Further addition of pyridine-$d_5$ up to 10 vol% provides well-defined resonances of all protons. Notably, the resonances of *ortho*-protons of pyridine moiety remains broadened even when all other signals become sharp, unless 10 vol% of pyridine-$d_5$ is present in the solution. These protons are expected to be the most sensitive to the self-assembly due to their proximity to the metal centres in the associates. Moreover, the signal of these protons is gradually shifted downfield along with the increase of pyridine-$d_5$ concentration that also testifies their location over the aromatic porphyrin macrocycle in the studied associates.

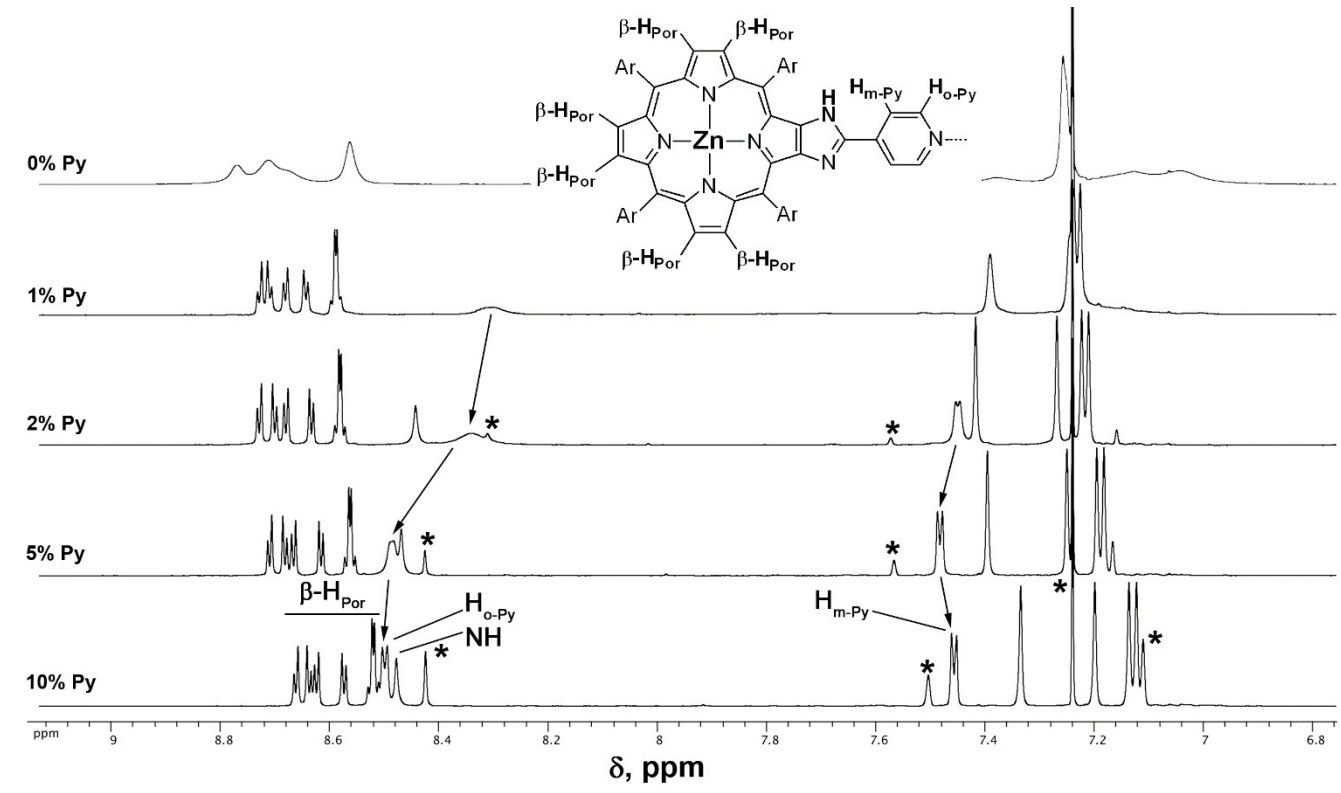


Figure 5. Aromatic regions of the $^1$H NMR spectra of **PyPorZn** upon variation of pyridine-$d_5$ amount in $CDCl_3$ (residual signals of $CDCl_3$ and pyridine-$d_5$ are marked with asterisk).

View Article Online
DOI: 10.1039/C8CE01992D

# Journal Name

## ARTICLE



Thus, it can be assumed that the introduction of pyridine-$d_5$ as a substituting ligand promotes the dissociation of oligomers of **PyPorZn** as shown in Scheme 2.

The self-assembly process was also investigated using temperature-dependent UV–Vis spectroscopy. First, the spectra of $10^{-4}$ M solution of complex **PyPorZn** in toluene were recorded at 1–95°C. Systematic changes in the Q bands region of the spectrum with the variation of the temperature are shown in Figure 6. As expected, the spectrum remains virtually unchanged in this temperature range when 1 vol% of pyridine is added to the studied solution because pyridine suppresses the self-assembly of the complex. Free-base porphyrin **PyPor** and nickel complex **PyPorNi** also do not reveal the temperature dependence of their UV–vis spectra (Figure S7). Altogether these observations could be reasonably explained by the dissociation of the **PyPorZn** associates at high temperatures.

The dependence of self-assembly of **PyPorZn** on the complex concentration in $CHCl_3$ was investigated in $5.40\cdot10^{-7}$–$1.08\cdot10^{-3}$ M concentration range. A significant and regular shift and a redistribution of intensities of the absorption bands were clearly observed along with the decrease of the complex concentration (Figure 7). At high concentrations two Q-bands, typical for metalloporphyrins, were observed in lower-energy region, while the Soret band was notably broadened. Dilution of the solution resulted in a gradual blue shift of the Q-bands as well as in narrowing and a blue shift of the Soret band. Gradual changes in the shape of the spectrum indicate that the association process is not completely suppressed even at minimal reached concentrations.

The observed stack of spectra did not reveal any isosbestic points, that testifies the presence of more than two absorbing species in the studied solution. It seems that the self-assembly of complex **PyPorZn** under these conditions leads to a mixture of oligomers, in contrast to the earlier reported aggregation of porphyrin **2PyZn** which affords dimeric species in chlorinated solvents. Noteworthy, the spectral changes observed along with dilution of this solution were identical to those appeared

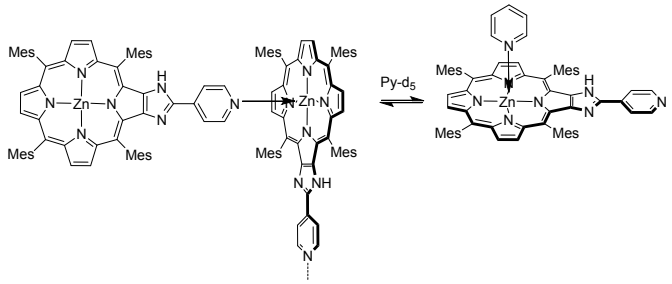


Scheme 2. Schematic representation of the ligand exchange observed in $CDCl_3$ solution of **PyPorZn** upon addition of pyridine-$d_5$.

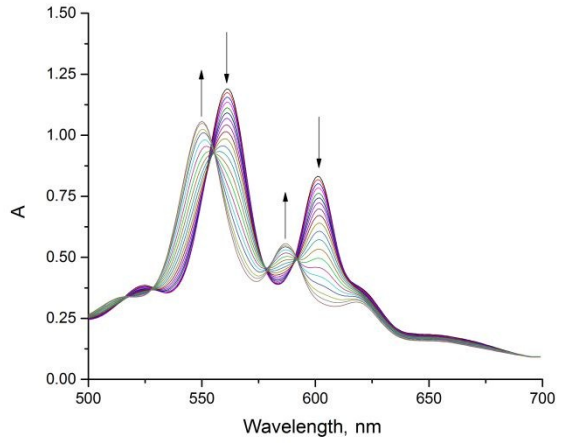


Figure 6. Evolution of the Q-bands region of UV–vis spectrum of **PyPorZn** in toluene at 1→95°C.

when the temperature of a toluene solution of the complex was increased.

Porphyrins **PyPor** and **PyPorNi** were also investigated under similar conditions and these studies revealed that UV–Vis spectra of both compounds remained virtually unchanged when their concentration was varied.

Considering the stack of the spectra obtained upon dilution of the $CHCl_3$ solution of **PyPorZn**, we have attempted to evaluate its association degree and the corresponding stability constants of self-assembled species. The calculations of the stability constants were performed by curve fitting procedure

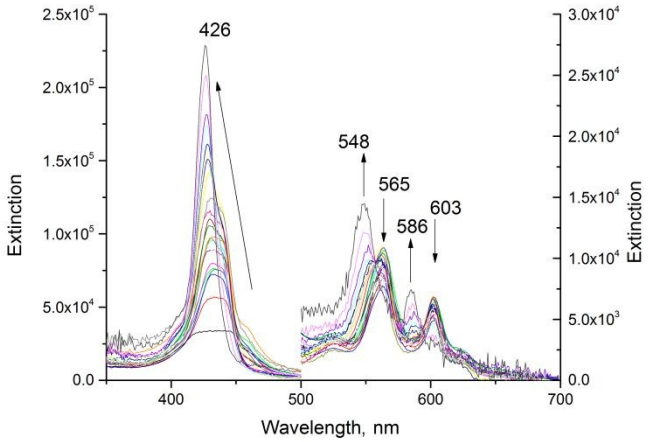


Figure 7. Evolution of UV–vis spectrum of **PyPorZn** in $CHCl_3$ upon dilution ($5.40\cdot10^{-7}$–$1.04\cdot10^{-3}$ M).

View Article Online
DOI: 10.1039/C8CE01992D

Journal Name

ARTICLE



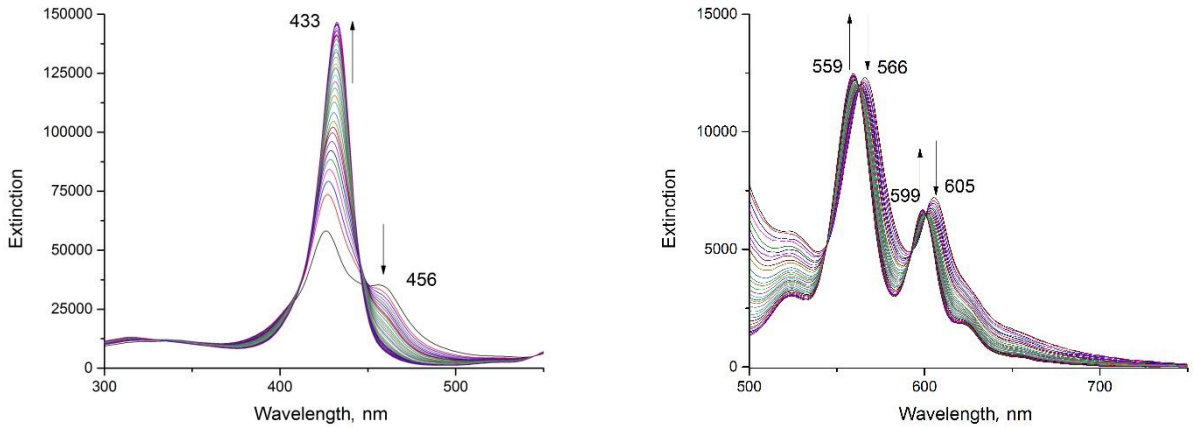


Figure 8. Evolution of UV–vis spectrum of **PyPorZn** in chloroform upon titration with $Ph_3PO$.

with ChemEqui 7.23 program package.[63] Unfortunately, all checked model systems provided a low accuracy of the calculations that indicates that a complicated set of equilibria exists in the studied solution and the calculation of the stability constants by using this technique is impossible due to the similarity of UV–vis spectra of self-assembled species.

The titration of **PyPorZn** with triphenylphosphine oxide in chloroform was also performed. Phosphine oxide being a competing ligand also suppresses the self-assembly of **PyPorZn** as can be clearly observed from the changes in UV–vis spectrum (Figure 8). However, the step-wise ligand addition (up to 300 equiv) did not allow to achieve a complete conversion of the self-assembled species to monomer complex **PyPorZn**···**OPPh$_3$**. Attempts of quantitative analysis of this titration data using ChemEqui 7.23 program were unsuccessful.

## Experimental

All chemicals were purchased from commercial suppliers, unless otherwise stated. The solvents have been purified according to conventional methods.[64] 2,3-Dioxo-5,10,15,20-tetramesitylchlorin was prepared according to the previously published procedure.[14,15] Chromatographic purifications were performed with Macherey-Nagel, Silica 60, 0.063-0.2 mm. Merck aluminum plates (TLC Silica 60 F254) were used for TLC analysis which were performed with dichloromethane as eluent.

$^1$H NMR spectra were recorded at Bruker Avance III spectrometer with 600 MHz proton frequency in $CDCl_3$ or $CDCl_3$/pyridine-$d_5$ mixtures at ca. $10^{-4}$ M at 303 K using the resonance of residual $CHCl_3$ as an internal reference ($\delta$ = 7.26 ppm). High-resolution mass-spectra were recorded with the use of Agilent 1260 chromatographic system (Agilent, USA) equipped with Bruker Maxis quadrupole and time-of-flight mass spectrometric detector (Bruker, Germany) with electrospray ionization (ESI) in positive ion mode. UV–vis spectra were recorded at Helios Alpha spectrophotometer (Thermo Scientific) in 250–900 nm range using rectangular quartz cells with 0.0882–10 mm optical path. Variable-temperature UV–vis measurements were performed in rectangular quartz cells with a 1 cm optical path using a Thermo Evolution 210 spectrometer equipped with Peltier thermostating accessory (Thermo Scientific PCCU1).

The measurements were made at the Shared Facility Centers of the Institute of Physical Chemistry and Electrochemistry RAS.

**X-ray diffraction experiment** was performed on a Bruker Kappa Apex II automatic four-circle diffractometer equipped with an area detector. The unit cell parameters were refined over the whole dataset.[65] The experimental reflection intensities were corrected for absorption using SADABS program[66] and the structure was solved by the direct method (SHELXS97)[67] and refined by the full-matrix least-squares method (SHELXL-2014)[68] on $F^2$ over the whole dataset in the anisotropic approximation for all nonhydrogen atoms. Olex2 was used as GUI for structure refinement.[69] The hydrogen atoms were placed in the geometrically calculated positions with the isotropic temperature factors equal to 1.2- (CH and NH groups) or 1.5-fold (Me group) equivalent isotropic temperature factor of the adjacent C or N atoms. The hydrogen atom on imidazole N(6) atom was located using the difference Fourier map and placed in the geometrically calculated position. SCXRD experiment and

refinement are detailed in the Supporting Information. Data CCDC 1871295 contain the supplementary crystallographic information for this paper. These data can be obtained free of charge from Cambridge Crystallographic Data Center via www.ccdc.cam.ac.uk/data request/cif.

The comparison of the crystal structure parameters with the analogous compounds were performed using ConQuest search in Cambridge Structural Database (CSD, Version 5.39).

**The analysis of crystal packing** was performed using ToposPro program package.[70] The molecular Voronoi-Dirichlet polyhedra (VDP) boundary surface between two molecules is appropriate characteristic to assess geometry and strength of the intermolecular interaction.[71] The boundary surface area of van der Waals contacts between porphyrin moieties was determined by the calculation of molecular VDP for each porphyrin molecule. The boundary surface between two porphyrins was considered meaningful if it was higher than the boundary surface between porphyrin and solvent (toluene) molecules (more than 70 Å$^2$). The most important contacts were chosen by the highest boundary surface. The distances between centers of the neighbouring porphyrin molecules and the values of boundary surfaces are shown in the Table S4. Standard simplification and determination of the topological type was performed considering the strongest contacts between porphyrins.

**All quantum chemistry computations** were performed with the Gaussian 09, Revision D.01 program[72] using the density functional theory (PBE0)[73] and the def-2-TZVP basis set. Topological analysis of the ρ(**r**) function, calculations of the v($\mathbf{r_{bcp}}$) and integration over interatomic zero-flux surfaces were performed using the AIMAll program.[74] All expected critical points were found and the whole set of critical points in each system satisfies the Poincaré-Hopf rule.

**UV–vis measurements**. Variable temperature UV–vis spectra were recorded in 470–700 nm range using a rectangular quartz cell with 1 cm optical path which was equipped with a teflon stopper and a magnetic stirring bar. The spectra were acquired in toluene at 1–95°C with the acquisition interval of 5°C. The solution was kept at each present temperature for 3 min to achieve the equilibrium state.

Variable concentration UV–vis measurements were performed by gradual dilution of $1.08\cdot10^{-3}$ M solution of **PyPorZn** in toluene to 1:2000, corresponding to $5.4\cdot10^{-7}$ M final concentration. The spectra were recorded in rectangular cells with optical paths of 0.0882 mm, 1 mm, 2 mm, 5 mm and 10 mm.

**Calculations of the stability constants** were performed by curve fitting procedure with ChemEqui 7.23 program package.[63] Maxima of the absorption bands at 426, 548, 565, 586 and 603 nm were used for numerical data adjustment. The approximation was performed using models of olygomers consisting of up to 5 molecular units with their stepwise dissociation processes considered. The analysis has revealed that the performed fitting gives high values of the Hamilton R-factor (20–40%) and also significant divergence of Logβ values determined by the evolution of different absorption bands.

**5,10,15,20-Tetramesityl-2-(4-pyridyl)-1*H*-imidazo[4,5-*b*] porphyrin (PyPor).** 4-Formylpyridine (33 mg, 29μL, 0.308 mmol, 5 eq), ammonium acetate (474 mg, 6.16 mmol, 100 eq) and trifluoroacetic acid (131 μL) were added to the solution of 2,3-dioxo-5,10,15,20-tetramesitylchlorin (50 mg, 0.0616 mmol) in chloroform (13 mL). The reaction mixture was refluxed and monitored by TLC. When starting compound was consumed (3 h), the reaction mixture was cooled to room temperature, washed with water (2 × 30 mL), dried over anhydrous sodium sulfate and evaporated under reduced pressure. The crude solid was purified by silica gel column chromatography using $CH_2Cl_2$/MeOH (0→0.5 vol.% of MeOH) mixture as an eluent. Porphyrin **PyPor** was obtained as a purple solid in 61% yield (34 mg).

$^1$H NMR ($CDCl_3$; δ, ppm; *J*, Hz): 8.88 (d, 1H, $^3J$=4.6, $H_\beta$), 8.82 (br.s, 2H, $H_\beta$), 8.77 (d, 1H, $^3J$=4.7, $H_\beta$), 8.72 (d, 2H, $^3J$=5.4, $H_{o\text{-Py}}$), 8.60 (s, 2H, $H_\beta$), 8.44 (s, 1H, $NH_{Imd}$), 7.56 (d, 2H, $^3J$=5.4, $H_{m\text{-Py}}$), 7.52 (s, 2H, $H_{Mes}$), 7.35 (s, 2H, $H_{Mes}$), 7.30 (s, 2H, $H_{Mes}$), 7.29 (s, 2H, $H_{Mes}$), 2.79 (s, 3H, $H_{p\text{-Me}}$), 2.71 (s, 3H, $H_{p\text{-Me}}$), 2.64 (s, 6H, $H_{p\text{-Me}}$), 1.89 (s, 6H, $H_{o\text{-Me}}$), 1.87 (s, 12H, $H_{o\text{-Me}}$), 1.86 (s, 6H, $H_{o\text{-Me}}$), 1.85 (s, 6H, $H_{o\text{-Me}}$), -2.69 (s, 2H, $NH_{Por}$). HR-MS (ESI): m/z calculated for $C_{62}H_{58}N_7$ $[M+H]^+$ 900.4754; found 900.4735. UV–vis ($CHCl_3$): $\lambda_{max}$, nm (log *ε*) 313 (4.12), 421 (5.28), 516 (4.08), 548 (3.69), 586 (3.69), 646 (3.24).

**5,10,15,20-Tetramesityl-2-(4-pyridyl)-1*H*-imidazo[4,5-*b*] porphyrinato nickel(II) (PyPorNi)**. The free-base **PyPor** (50 mg, 0.052 mmol) and $Ni(acac)_2\times H_2O$ (26.7 mg, 0.104 mmol, 2 eq) were refluxed in toluene (10 ml) for 2 h and the reaction progress was monitored by TLC. After complete consumption of the starting material the reaction mixture was cooled to ambient temperature, evaporated to minimal volume and the residue was passed through a 5 cm silica pad with hexane/dichloromethane (1:1) mixture as an eluent. The evaporation of the obtained coloured fraction provided 47 mg (95%) of **PyPorNi** (purity *ca*. 95%) as a red solid.

$^1$H NMR ($CDCl_3$; δ, ppm; *J*, Hz): 8.72 (s, 2H, $H_{o\text{-Py}}$), 8.68 (d, 1H, $^3J$=4.4, $H_\beta$), 8.63-8.66 (2d, 2H, $^3J$=4.4, $H_\beta$), 8.59 (d, 1H, $^3J$=4.4, $H_\beta$), 8.52-8.57 (m, 2H, $H_\beta$), 8.47 (s, 1H, $NH_{Imd}$), 7.54-7.57 (br.d, 2H, $H_{m\text{-Py}}$), 7.43 (s, 2H, $H_{Mes}$), 7.27 (s, 2H, $H_{Mes}$), 7.22 (s, 2H, $H_{Mes}$), 7.21 (s, 2H, $H_{Mes}$), 2.72 (s, 3H, $H_{p\text{-Me}}$), 2.64 (s, 3H, $H_{p\text{-Me}}$), 2.58 (s, 6H, $H_{p\text{-Me}}$), 1.85 (s, 6H, $H_{o\text{-Me}}$), 1.84 (s, 6H, $H_{o\text{-Me}}$), 1.82 (s, 6H, $H_{o\text{-Me}}$), 1.79 (s, 6H, $H_{o\text{-Me}}$). HR-MS (ESI): m/z calculated for $C_{62}H_{56}N_7Ni$ $[M+H]^+$ 956.3945, found 956.3952. UV–vis ($CHCl_3$): $\lambda_{max}$, nm (log *ε*) 321 (4.13), 419 (5.19), 529 (4.01), 566 (3.81).

**5,10,15,20-Tetramesityl-2-(4-pyridyl)-1H-imidazo[4,5-b] porphyrinato zinc(II) (PyPorZn)**. The free-base **PyPor** (39 mg, 0.043 mmol) and $Zn(OAc)_2$ (16 mg, 0.086 mmol, 2 eq) were stirred in a mixture of chloroform (6.2 ml) and methanol (1.6 ml) at ambient temperature overnight. The formed precipitate was filtered, washed with methanol and dried in air providing the resulting **PyPorZn** as a violet solid in 95% yield (39 mg).

$^1$H NMR ($CDCl_3$ + 10 % pyridine-$d_5$; δ, ppm; *J*, Hz): 8.66 (d, 1H, $^3J$=4.5, $H_\beta$), 8.64 (d, 1H, $^3J$=4.4, $H_\beta$), 8.62 (d, 1H, $^3J$=4.4, $H_\beta$), 8.57 (d, 1H, $^3J$=4.5, $H_\beta$), 8.53 (d, 1H, $^3J$=4.5, $H_\beta$), 8.51 (d, 1H, $^3J$=4.5, $H_\beta$), 8.50 (d, 2H, $^3J$=5.5, $H_{m\text{-Py}}$), 8.48 (s, 1H, $NH_{Imd}$), 7.46 (d, 2H, $^3J$=5.6, $H_{o\text{-Py}}$), 7.34 (s, 2H, $H_{Mes}$), 7.20 (s, 2H, $H_{Mes}$), 7.14 (s, 2H, $H_{Mes}$), 7.12 (s, 2H, $H_{Mes}$), 2.63 (s, 3H, $H_{p\text{-Me}}$), 2.57 (s, 3H, $H_{p\text{-Me}}$), 2.49 (s, 3H, $H_{p\text{-Me}}$), 2.48 (s, 3H, $H_{p\text{-Me}}$), 1.72 (s, 6H, $H_{o\text{-Me}}$), 1.70 (s, 12H, $H_{o\text{-Me}}$), 1.68 (s, 6H, $H_{o\text{-Me}}$). HR-MS (ESI): m/z calculated for

View Article Online DOI: 10.1039/C8CE01092D



$C_{62}H_{56}N_7Zn$ $[M+H]^+$ 962.3810, found 962.3845. UV–vis ($CHCl_3$+1%Py): $\lambda_{max}$, nm (log ε) 316 (4.41), 434 (5.32), 523 (3.63), 561 (4.26), 601 (3.99).

## Conclusions

To study the self-assembly of imidazoporphyrins, 5,10,15,20-tetramesityl-2-(4-pyridyl)-1*H*-imidazo[4,5-*b*]porphyrin (**PyPor**) bearing a 4-pyridine donor site separated from the porphyrin macrocycle by a rigid imidazole linker was designed and synthesized in high yield by the condensation of the corresponding 2,3-dioxochlorin and 4-formylpyridine in the presence of ammonium acetate. The corresponding zinc and nickel complexes were also prepared in high yields.

Zinc complex **PyPorZn** was characterized by single-crystal X-ray diffraction. This complex crystallizes with two toluene molecules forming 1D coordination polymer through the axial coordination of the pyridine nitrogen atom to the zinc atom of the neighbouring porphyrin molecule. Significant deviation of the pyridine ring from the expected orthogonal orientation with respect to the macrocycle plane is observed. This unusual orientation was analysed by DFT PBE0 calculations of zinc 5,10,15,20-tetraphenylporphyrinate with an axial pyridine molecule (**TPPZn–Py**) as a model compound. According to these calculations, the energy decrease of the Zn–$N_{Py}$ bond induced by the tilt of the pyridine fragment in the coordination sphere of the zinc atom is small. This peculiarity may be observed in polymer chains **[PyPorZn]$_n$** due to the increase of energy of multiple weak interactions in the crystals caused by this tilting.

Being dissolved in weakly coordinating solvents, complex **PyPorZn** exists as a mixture of oligomers. This first example of self-assembled imidazoporphyrins shows the prospects of such easily accessible β-substituted porphyrins in which a donor site lies on the $C_2$ axis of the macrocycle for biomimetic studies. These compounds are promising models of native tetrapyrrole macrocycles and building blocks for the elaboration of functional molecular materials. These ongoing studies will be reported soon.

## Conflicts of interest

There are no conflicts to declare.

## Acknowledgements

This work was supported by the RAS, the Russian Foundation for Basic Research (grant N 17-53-16025), CNRS and was carried out in the framework of the International Associated French–Russian Laboratory of Macrocyclic Systems and Related Materials (LIA LAMREM). Abdulaeva I.A. thanks the French government for the PhD fellowship. The analysis of crystal structures in ToposPro was performed with the support of the Russian Science Foundation (grant # 18-73-00246) and with the help of Dr. Alexandrov E.V. (Samara State University) in structure simplification. K.A. Lyssenko is grateful to the Russian Science Foundation (grant # 14-13-00884) for financial support of DFT calculations and analysis of electron density topology.

## Notes and references


1 M. G. H. Vicente, in *The Porphyrin Handbook*, eds. K. M. Kadish, K. M. Smith and R. Guilard, Academic Press, 2000, p. 149.

2 L. Jaquinod, in *The Porphyrin Handbook*, eds. K. M. Kadish, K. M. Smith and R. Guilard, Academic Press, 2000, p. 201.

3 K. P. Ghiggino, J. A. Hutchison, D.-M. Shafiqul Islan, Y. Araki, O. Ito, S. J. Langford, V.-L. Lau and M. Takezaki, *Photochem. Photobiol. Sci.*, 2006, **5**, 1150–1153.

4 H. Jia, B. Schmid, S. X. Liu, M. Jaggi, P. Monbaron, S. V. Bhosale, S. Rivadehi, S. J. Langford, L. Sanguinet, E. Levillain, M. E. El-Khouly, Y. Morita, S. Fukuzumi and S. Decurtins, *Chem. Phys. Chem*, 2012, **13**, 3370–3382.

5 H. Hayashi, A. S. Touchy, Y. Kinjo, K. Kurotobi, Y. Toude, S. Ito, H. Saarenpaa, N. V. Tkachenko, H. Lemmetyinen and H. Imahori, *ChemSusChem*, 2013, **6**, 508–517.

6 J. Rubio-Magnieto, F. Di Meo, M. Lo, C. Delcourt, S. Clement, P. Norman, S. Richeter, M. Linares and M. Surin, *Org. Biomol. Chem.*, 2015, **13**, 2453–2463.

7 M. Abdelhameed, P. L. Karsenti, A. Langlois, J. F. Lefebvre, S. Richeter, R. Ruppert and P. D. Harvey, *Chem. – A Eur. J.*, 2014, **20**, 12988–13001.

8 J. F. Longevial, A. Langlois, A. Buisson, C. H. Devillers, S. Clement, A. Van Der Lee, P. D. Harvey and S. Richeter, *Organometallics*, 2016, **35**, 663–672.

9 J.-F. Lefebvre, M. Lo, D. Leclercq and S. Richeter, *Chem. Commun.*, 2011, **47**, 2976–8.

10 J.-F. F. Lefebvre, D. Leclercq, J.-P. P. Gisselbrecht and S. Richeter, *Eur. J. Org. Chem.*, 2010, 1912–1920.

11 M. Lo, J.-F. Lefebvre, D. Leclercq, A. van der Lee and S. Richeter, *Org. Lett.*, 2011, **13**, 3110–3113.

12 J. F. Lefebvre, M. Lo, J. P. Gisselbrecht, O. Coulembier, S. Clement and S. Richeter, *Chem. – A Eur. J.*, 2013, **19**, 15652–15660.

13 J.-F. F. Lefebvre, J.-F. F. Longevial, K. Molvinger, S. Clément, S. Richeter, S. Clement, S. Richeter, S. Clement and S. Richeter, *C. R. Chim.*, 2016, **19**, 94–102.

14 M. J. Crossley and J. A. Mcdonald, *J. Chem. Soc. Perkin Trans. 1*, 1999, 2429–2431.

15 I. A. Abdulaeva, K. P. Birin, J. Michalak, A. Romieu, C. Stern, A. Bessmertnykh-Lemeune, R. Guilard, Y. G. Gorbunova and A. Y. Tsivadze, *New J. Chem.*, 2016, **40**, 5758–5774.

16 I. A. Abdulaeva, K. P. Birin, Y. G. Gorbunova, A. Y. Tsivadze and A. Bessmertnykh-Lemeune, *J. Porphyr. Phthalocyanines*, 2018, **22**, 619–631.

17 K. P. Birin, A. I. Poddubnaya, I. A. Abdulaeva, Y. G. Gorbunova and A. Y. Tsivadze, *DyesPigm*, 2018, **156**, 243–249.

18 Y. Kashiwagi, K. Ohkubo, J. A. McDonald, I. M. Blake, M. J. Crossley, Y. Araki, O. Ito, H. Imahori and S. Fukuzumi, *Org. Lett.*, 2003, **5**, 2719–2721.

19 M. Yu, S. Wang, K. Feng, T. Khoury, M. J. Crossley, F. Yang, J. Zhang, C. Tung and L. Wu, *J. Phys. Chem. C*, 2011, **115**,

23634–23641.
20 D. Curiel, K. Ohkubo, J. R. Reimers, S. Fukuzumi and M. J. Crossley, *Phys. Chem. Chem. Phys.*, 2007, **9**, 5260.
21 S.-H. Lee, A. G. Larsen, K. Ohkubo, Z.-L. Cai, J. R. Reimers, S. Fukuzumi and M. J. Crossley, *Chem. Sci.*, 2012, **3**, 257–269.
22 S. P. Gaynor, M. J. Gunter, M. R. Johnston and R. N. Warrener, *Org. Biomol. Chem.*, 2006, **4**, 2253–2266.
23 Y. Y. Enakieva, A. G. Bessmertnykh, Y. G. Gorbunova, C. Stern, Y. Rousselin, A. Y. Tsivadze and R. Guilard, *Org. Lett.*, 2009, **11**, 3842–3845.
24 A. Lemeune, A. Y. Mitrofanov, Y. Rousselin, C. Stern, R. Guilard, Y. Y. Enakieva, Y. G. Gorbunova and S. E. Nefedov, *Phosphorus. Sulfur. Silicon Relat. Elem.*, 2015, **190**, 831–836.
25 E. V. Vinogradova, Y. Y. Enakieva, S. E. Nefedov, K. P. Birin, A. Y. Tsivadze, Y. G. Gorbunova, A. G. Bessmertnykh Lemeune, C. Stern and R. Guilard, *Chem. – A Eur. J.*, 2012, **18**, 15092–15104.
26 A. A. Sinelshchikova, S. E. Nefedov, Y. Y. Enakieva, Y. G. Gorbunova, A. Y. Tsivadze, K. M. Kadish, P. Chen, A. Bessmertnykh-Lemeune, C. Stern and R. Guilard, *Inorg. Chem.*, 2013, **52**, 999–1008.
27 Y. Y. Enakieva, M. V. Volostnykh, S. E. Nefedov, G. A. Kirakosyan, Y. G. Gorbunova, A. Y. Tsivadze, A. G. Bessmertnykh-Lemeune, C. Stern and R. Guilard, *Inorg. Chem.*, 2017, **56**, 3055–3070.
28 K. P. Birin, Y. G. Gorbunova, A. Y. Tsivadze, A. G. Bessmertnykh-Lemeune and R. Guilard, *Eur. J. Org. Chem.*, 2015, 5610–5619.
29 I. Beletskaya, V. S. Tyurin, A. Y. Tsivadze, R. Guilard and C. Stern, *Chem. Rev.*, 2009, **109**, 1659–1713.
30 Y. Kobuke, in *Structure and bonding*, Springer-Verlag, Berlin/Heidelberg, 2006, pp. 49–104.
31 M. Morisue and Y. Kobuke, in *Handbook of Porphyrin Science*, eds. K. M. Kadish, K. M. Smith and R. Guilard, World Scientific: Singapore, 2014, pp. 1–126.
32 X. Rui, Q.-Z. Zha, T.-T. Wei and Y.-S. Xie, *Inorg. Chem. Commun.*, 2014, **48**, 111–113.
33 S. Goswami, B. K. Tripuramallu and I. Goldberg, *CrystEngComm*, 2017, **19**, 6845–6857.
34 W. Xu, Z. Zhang, X. Zhao and J. Li, *J. Coord. Chem.*, 2017, **70**, 746–755.
35 N. Marets, V. Bulach and M. W. Hosseini, *New J. Chem.*, 2013, **37**, 3549.
36 V. Bulach and M. W. Hosseini, in *Handbook of Porphyrin Science*, 2011, pp. 299–390.
37 F. Sguerra, V. Bulach and M. W. Hosseini, *Dalt. Trans.*, 2012, **41**, 14683.
38 E. Deiters, V. Bulach and M. W. Hosseini, *New J. Chem.*, 2006, **30**, 1289.
39 E. Kuhn, V. Bulach and M. W. Hosseini, *Chem. Commun.*, 2008, 5104.
40 R. T. Stibrany, J. Vasudevan, S. Knapp, J. A. Potenza, T. Emge and H. J. Schugar, *J. Am. Chem. Soc.*, 1996, **118**, 3980–3981.
41 A. G. Bessmertnykh-Lemeune, R. Guilard, C. Stern, Y. Y. Enakieva, Y. G. Gorbunova, A. Y. Tsivadze and S. E. Nefedov, in *Supramolecular Systems: Chemistry, Types and Applications*, ed. C. Pena, Nova Science, 2016.
42 Y. Shinozaki, I. Yoshikawa, K. Araki, K. Sugawa and J. Otsuki, *Cryst. Eng Commun.*, 2014, **16**, 9155–9157.
43 E. B. Fleischer and A. M. Shachter, *Inorg. Chem.*, 1991, **30**, 3763–3769.
44 T. S. Balaban, R. Goddard, M. Linke-Schaetzel and J.-M. Lehn, *J. Am. Chem. Soc.*, 2003, **125**, 4233–4239.
45 C. Xia, C. Lu, X. Wu, L. Chen, Q. Zhang, J. Zhang and D. Wu, *Inorganica Chim. Acta*, 2006, **359**, 4639–4644.
46 I. Elguraish, K. Zhu, L. A. Hernandez, H. Amarne, J. Luo, V. N. Vukotica and S. J. Loeb, *Dalt. Trans.*, 2015, **44**, 898–902.
47 A. Tsuda, T. Nakamura, S. Sakamoto, K. Yamaguchi and A. Osuka, *Angew. Chem. Int. Ed.*, 2002, **41**, 2817–2821.
48 A. Ozarowski, H. M. Lee and A. L. Balch, *J. Am. Chem. Soc.*, 2003, **125**, 12606–12614.
49 D. V Konarev, A. L. Litvinov, I. S. Neretin, N. V Drichko, Y. L. Slovokhotov, R. N. Lyubovskaya, J. A. K. Howard and D. S. Yufit, *Cryst. Growth Des.*, 2004, **4**, 643–646.
50 Y. Diskin-Posner, G. K. Patra and I. Goldberg, *Dalt. Trans.*, 2001, **2**, 2775–2782.
51 R. W. Seidel, R. Goddard, K. Focker and I. M. Oppel, *CrystEngComm*, 2010, **12**, 387–394.
52 A. R. Mulholland, P. Thordarson, E. J. Mensforth and S. J. Langford, *Org. Biomol. Chem.*, 2012, **10**, 6045–6053.
53 M. G. Medvedev, I. S. Bushmarinov, J. Sun, J. P. Perdew and K. A. Lyssenko, *Science (80-. ).*, 2017, **355**, 49–52.
54 S. Grimme, J. Antony, S. Ehrlich and H. Krieg, *J. Chem. Phys.*, 2010, **132**, 154104.
55 S. Grimme, S. Ehrlich and L. Goerigk, *J. Comput. Chem.*, 2011, **32**, 1456–1465.
56 C. F. Matta and R. J. Boyd, *The Quantum Theory of Atoms in Molecules: from Solid State to DNA and Drug Design*, Wiley-VCH Verlag GmbH & Co. KgaA, Weinheim, 2007.
57 E. Espinosa, E. Molins and C. Lecomte, *Chem. Phys. Lett.*, 1998, **285**, 170–173.
58 I. V. Ananyev, V. A. Karnoukhova, A. O. Dmitrienko and K. A. Lyssenko, *J. Phys. Chem. A*, 2017, **121**, 4517–4522.
59 L. N. Puntus, K. A. Lyssenko, M. Y. Antipin and J. C. G. Bünzli, *Inorg. Chem.*, 2008, **47**, 11095–11107.
60 A. O. Borissova, A. A. Korlyukov, M. Y. Antipin and K. A. Lyssenko, *J. Phys. Chem. A*, 2008, **112**, 11519–11522.
61 S. Z. Vatsadze, A. V. Medved'ko, N. V Zyk, A. L. Maximov, S. A. Kurzeev, G. M. Kazankov and K. A. Lyssenko, *Organometallics*, 2009, **28**, 1027–1031.
62 A. O. Borissova, M. Y. Antipin, D. S. Perekalin and K. A. Lyssenko, *CrystEngComm*, 2008, **10**, 827–832.
63 V. P. Solovev, *http://vpsolovev.ru/programs/chemequi/*.
64 W. L. F. Armarego and C. L. L. Chai, *Purification of laboratory chemicals*, Elsevier/Butterworth-Heinemann, 2009.
65 *Bruker (2012). SAINT-Plus, Version 7.68. Bruker AXS Inc., Madison, Wisconsin, USA*.
66 *Bruker (2001). SADABS. Bruker AXS Inc., Madison, Wisconsin, USA.*
67 G. M. Sheldrick, *Acta Cryst. A*, 2007, **64**, 112–122.
68 G. M. Sheldrick, *Acta Cryst. C*, 2015, **71**, 3–8.

View Article Online
DOI: 10.1039/C8CE01992D

69 O. V Dolomanov, L. J. Bourhis, R. J. Gildea, J. A. K. Howard and H. Puschmann, *J.Appl.Cryst.*, 2009, **42**, 339–341.
70 V. A. A. Blatov, A. P. P. Shevchenko and D. M. M. Proserpio, *Cryst. Growth Des.*, 2014, **14**, 3576–3586.
71 V. A. Blatov, *Crystallogr. Rev.*, 2004, **10**, 249–318.
72 D. J. F. M. J. Frisch, G. W. Trucks, H. B. Schlegel, G. E. Scuseria, M. A. Robb, J. R. Cheeseman, G. Scalmani, V. Barone, G. A. Petersson, H. Nakatsuji, X. Li, M. Caricato, A. Marenich, J. Bloino, B. G. Janesko, R. Gomperts, B. Mennucci, H. P. Hratchian, J. V. Ort, *Gaussian 09, Revision D.01*, Gaussian, Inc., Wallingford CT, 2016.
73 J. P. Perdew, M. Ernzerhof and K. Burke, *J. Chem. Phys.*, 1996, **105**, 9982–9985.
74 T. Keith, *AIMAll ver. 16.08.17*.